applied sciences

MDPI

Article

Influence of Non-Ionic Surfactant and Silver on the Photocatalytic Activity of TiO_2 Films for Degradation of Dyes in Distilled and Tap Water

Dobrina Ivanova [1], Elisaveta Mladenova [2] and Nina Kaneva [1,*]

[1] Laboratory of Nanoparticle Science and Technology, Department of General and Inorganic Chemistry, Faculty of Chemistry and Pharmacy, University of Sofia, 1 James Bourchier Blvd., 1164 Sofia, Bulgaria; dobrina.k.ivanova@gmail.com

[2] Laboratory of Atomic-Absorption Spectrometry, Department of Analytical Chemistry, Faculty of Chemistry and Pharmacy, University of Sofia, 1 James Bourchier Blvd., 1164 Sofia, Bulgaria; elimladenova@chem.uni-sofia.bg

* Correspondence: nina_k@abv.bg

Abstract: This study describes the impact of surfactant molecular weights (PEG 2000 and PEG 4000) on the photocatalytic activity of TiO_2 films, deposited via dip-coating from a PEG-stabilized suspension and silver-functionalized photo-fixation of Ag^+ under UV illumination. The photocatalytic activity of pure and Ag/TiO_2 films is assessed in the aqueous-phase degradation of Malachite green and Methylene blue in distilled and tap water under UV and visible illumination. The results indicate a positive effect of both the higher-molecular-weight non-ionic surfactant and Ag-functionalization yield higher photocatalytic efficiency. Notably, films photo-fixed with 10^{-2} M Ag^+ show the highest degradation percentages in all experimental conditions. A direct correlation between the concentration of Ag^+ ions and the enhancement of the photocatalytic activity is revealed: pure TiO_2 < Ag, $10^{-4}/TiO_2$ < Ag, $10^{-3}/TiO_2$ < Ag, $10^{-2}/TiO_2$. Flame atomic absorption spectrometry is used to study the Ag^+ leeching from the Ag/TiO_2 films. The structural properties of the nanostructures are investigated through scanning electron microscopy, Brunauer–Emmett–Teller analysis, energy-dispersive X-ray spectroscopy, and X-ray diffraction. Additionally, after three cycles of operation, Ag, $10^{-2}/TiO_2$ (PEG 4000) films can maintain their photocatalytic activity, suggesting a potential application in the treatment of dye wastewater.

Keywords: Ag/TiO_2 powder films; non-ionic surfactant; organic dyes; tap water

check for updates

Citation: Ivanova, D.; Mladenova, E.; Kaneva, N. Influence of Non-Ionic Surfactant and Silver on the Photocatalytic Activity of TiO_2 Films for Degradation of Dyes in Distilled and Tap Water. *Appl. Sci.* **2024**, *14*, 4571. https://doi.org/10.3390/app14114571

Academic Editors: Fabrizio Medici and Laura Maria Raimondi

Received: 19 April 2024
Revised: 23 May 2024
Accepted: 24 May 2024
Published: 26 May 2024

Copyright: © 2024 by the authors. Licensee MDPI, Basel, Switzerland. This article is an open access article distributed under the terms and conditions of the Creative Commons Attribution (CC BY) license (https://creativecommons.org/licenses/by/4.0/).

1. Introduction

The high activity of photocatalysts has rendered them attractive materials for pollutant removal and recycling waste substances in the environment [1–4]. Despite the utilization of chemical precipitation, biological, and physical methods in wastewater treatment, they suffer from drawbacks, e.g., high costs and energy consumption, secondary waste generation, and prolonged treatment durations [5,6]. Consequently, alternative strategies must be devised to circumvent these limitations. Heterogeneous photocatalysis emerges as a viable solution due to its high effectiveness at mild conditions, governed by the production of reactive oxidative species ($OH^•$) [7]. TiO_2 stands out as a significant photocatalyst among various semiconductors owing to its exceptional activity and physicochemical properties crucial for pollutant remediation [8,9] but suffers from a general low quantum yield. Doping TiO_2 with non-metals, metals, and transition metals has been a strategy to enhance its photocatalytic performance [10–12]. Silver, in particular, shows promise in augmenting the physicochemical properties of TiO_2, offering potential applications in purification, antibacterial properties, and self-cleaning [13–15]. Saravanan et al. demonstrated that Ag-doped TiO_2 exhibits superior physicochemical properties compared to those of

TiO_2 [16]. Their findings reveal that Ag doping enhances the material's ability to absorb visible light, resulting in a narrower bandgap, reduced total surface area, and Ag surface plasmon resonance. Additionally, Chakhtouna et al. have explored Ag-TiO_2 photocatalysts for photocatalytic removal [17].

On the other hand, considerable effort has been dedicated to developing composite photocatalysts with surfactant assistance by employing structure modifiers to enhance their physicochemical and photocatalytic characteristics [18]. Surfactants such as polyvinylpyrrolidone, polyethylene glycol, and cetyltrimethylammonium bromide are commonly used in the synthesis of TiO_2 composites [19–22]. Among these, the non-ionic surfactant PEG is deemed an appropriate structure-directing agent due to its high water solubility, stability, non-toxicity, and thermal breakdown upon calcination [23,24]. PEG has been extensively researched for creating dye-sensitized TiO_2 nanoparticles to enhance stability, durability, and charge transfer during the energy production process [25,26]. Hu et al. [25] and An et al. [27] demonstrated that the morphology, crystalline size, and grain growth of PEG/TiO_2 photocatalysts are all highly influenced by the molecular weight of PEG, illustrating how the optimal molecular chain length could be of nanoparticle size and growth rate. Thus, incorporating PEG with optimum molecular weights to modify the unique Ag/TiO_2 photocatalyst may improve its morphology, crystalline structure, and catalytic activity under light irradiation.

In the current study, TiO_2 powder films are prepared using PEG with different molecular masses. The relationship between the physicochemical properties and the photocatalytic efficiency of the samples is evaluated. Our work focuses on: (i) the effects of PEG molecular mass on the structural and photocatalytic properties of TiO_2 powder films for accelerated organic dye degradation; (ii) the influence of silver ion concentrations, photo-fixed onto the film surface; (iii) the difference in the reactivity between the investigated pollutants; (iv) the photostability of TP4 and Ag, 10^{-2}/TP4 films after three cycle of photocatalysis; and (v) atomic-absorption determination of residual noble metal in dye solution.

2. Materials and Methods

TiO_2 commercial powder (≥99.0%), Polyethyleneglycol 2000 (PEG 2000), Polyethyleneglycol 4000 (PEG 4000), C_2H_5OH (≥99.0%), $AgNO_3$, and HNO_3 (≥69.0%) were obtained from Fluka (Buchs, Switzerland). Glass substates (76 × 26 × 1 mm) were supplied by ISO-LAB (Schweitenkirchen, Germany). Silver standard solution for FAAS 1000 mg/L (Sigma-Aldrich Chemie GmbH, Taufkirchen, Germany) and double-deionized water (Millipore purification system Synergy, France) was used for the preparation of FAAS calibration standard solutions.

For the photocatalytic tests, commercially available Malachite green oxalate (MG, λ_{max} = 615 nm, Croma-Gesellschaft mbH & Co.) and Methylene Blue (MB, λ_{max} = 660 nm, Fluka) were selected as model contaminants. Both distilled and tap (drinking) water were utilized in the photocatalytic tests to simulate pollutant degradation as it occurs in natural water systems. Tap water was obtained from Sofia municipal water supply and was of naturally low hardness (Na^+ < 5.01 mg/L, Ca^{2+} < 10.74 mg/L, Cl^- < 5 mg/L, NO_3^- < 0.94 mg/L, etc.).

The powder catalysts were prepared as follows: PEG (M_W 2000 or 4000) was dissolved in 50 mL ethanol (to obtain 14 wt%) under magnetic stirring at 70 °C, until a clear solution was obtained. The starting commercial TiO_2 powder was also suspended in 60 mL for 15 min at 23 ± 2 °C (to obtain 7 wt%) for 15 min at 23 ± 2 °C. The resulting dispersion was mixed with the PEG–ethanol solution, sonicated (15 kHz) for 30 min, and magnetically stirred for an additional 15 min to obtain the suspension used for TiO_2 depositions.

The glass slide substrates were coated employing a dip-coating technique performed at room temperature at a withdrawal rate of 0.9 cm/min. A total of five coating cycles were applied. After each coating cycle, the samples were dried at 100 °C for 2 min and finally annealed for one hour at 500 °C to burn off the organic material. The resulting TiO_2 films had a loading of 38.5 mg, covering an area of about 35 cm^2 (≈1.1 mg/cm^2). The

films obtained from two stabilizers, PEG 2000, and PEG 4000, are denoted as TP2 and TP4, respectively. The coating procedure is illustrated in Figure 1.

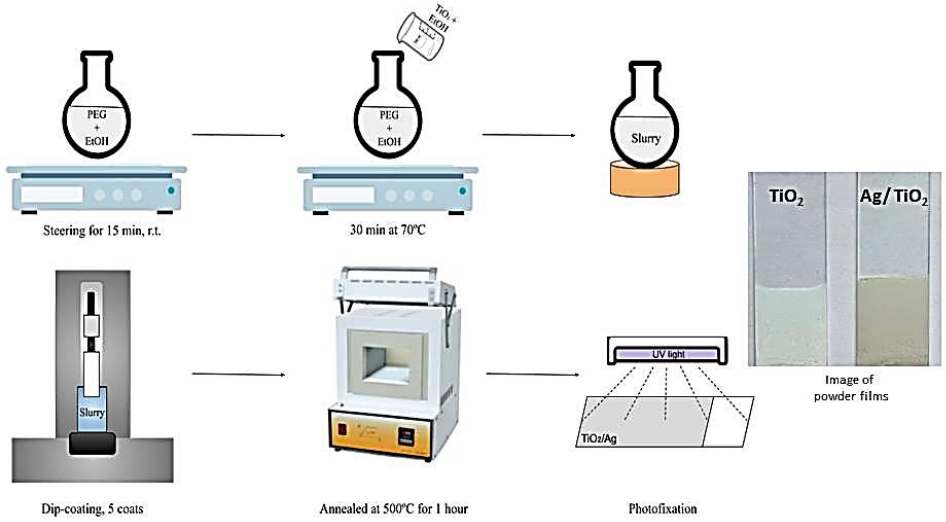

Figure 1. Schematic process for the preparation of TiO_2 and Ag/TiO_2 films.

To produce silver co-catalytically modified TiO_2 films, photo-deposition was employed. The Ag/TiO_2 films were photo-fixed by immersion in 10^{-2} M aqueous $AgNO_3$ for 20 min, followed by UV light exposure and rinsing with water (Figure 1). Subsequently, the Ag-modified films were dried for ten minutes at 100 °C to remove nitrate ions. These films were denoted as Ag, 10^{-2}/TP2 and Ag, 10^{-2}/TP4 for the films obtained from the PEG 2000 stabilizer and PEG 4000 stabilizer, respectively. To study the effects of the Ag-photodeposition solution concentration, additional films were prepared via the same procedure, but in 10^{-3} and 10^{-4} M $AgNO_3$ solutions, denoted as Ag, 10^{-3}/TP2 and Ag, 10^{-4}/TP2 for the PEG 2000-derived samples, and Ag, 10^{-3}/TP4, and Ag, 10^{-4}/TP4 for the PEG 4000-derived films, respectively.

The morphology of the samples was examined by SEM (Hitachi TM4000, 15 kV, Krefeld, Germany). The specific surface areas were measured using at low-temperature nitrogen adsorption (−196 °C) with a Quantachrome NOVA 1200e instrument. Energy-dispersive X-ray spectroscopy with a Bruker AXS detector (Microanalysis GmbH, Berlin, Germany) was used to determine the elemental composition.

X-ray diffractometer (Siemens D500 with CuKα radiation, Karlsruhe, Germany) was employed for XRD analysis of pure, Ag/TP2, and Ag/TP4 powder films to investigate the crystalline structure.

The aqueous-phase degradation of MG and MB gauged the photocatalytic activity of powder films at an initial dye concentration of 10 ppm. A 200 mL photoreactor, equipped with UV (36 W, 315–400 nm emission range) and visible (150 W LED, V-Tac, emitting 5700 K white, 420–700 nm) lamps, along with a magnetic stirrer (500 rpm) was used for the photocatalytic tests. Experiments were conducted at 23 ± 2 °C. The concentration of MG and MB, as a function of irradiation time, was estimated from absorbance measurements at 615 and 666 nm, respectively, on an UV–vis spectrophotometer (Evolution 300 Thermo Scientific (Madison, WI, USA) with a calibration curve. The data were converted into dye removal rate constants via the widely used $\ln(C/C_0)$ pseudo-first-order rate dependence.

Residual silver, released by Ag(I) leeching from the catalysts, was measured via a Flame Atomic Absorption Spectrometer (FAAS) on Perkin and Elmer AAnalyst spectrometer, equipped with a hollow cathode Ag lamp and air/acetylene. Calibration was performed at three concentrations of water standard solutions: 0.1, 0.5, and 1.0 mg/L, at an RSD of 2–4%. Sample solutions, taken from the dye aqueous phase during experiments, were concentrated 5-fold according to a previously developed procedure [28].

The total organic carbon in the treated dye solutions was measured using an Elementar Vario Select TOC analyzer (Langenselbold, Germany), based on catalytic oxidation. All measurements were performed in triplicates.

3. Results and Discussion

3.1. Structural Characterization

SEM images reveal a homogeneous surface morphology in all powder films, characterized by particles of varying sizes (Figure 2). This agglomeration is caused by the high temperature during sample preparation, inevitable for nanostructure formation.

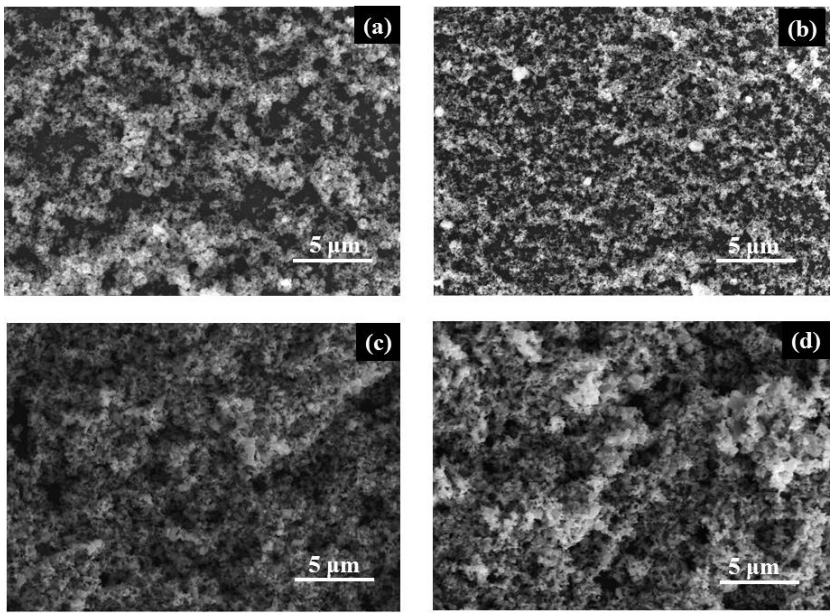

Figure 2. SEM images of (**a**) TP2, (**b**) Ag/TP2, (**c**) TP4, and (**d**) Ag/TP4 films.

Figure 2a,c depict the surface morphology of pure TP2 and TP4 films. It is evident that the morphology, crystalline size, and grain growth improve with increasing molecular weight of the surfactant. Co-catalytic modification with Ag^+ (10^{-2} M) shows minimal alteration to the surface of the original TiO_2 films (TP2 and TP4) with a slight reduction in crystal size, consistent with the XRD analysis. The reduced particle size in Ag/TiO_2 films may be attributed to the effect of electron confinement, which prevents surface Plasmon resonance from interacting with light. Tsivadze A. et al.'s explanation of this phenomenon can be linked to electronic barrier sets for Ag with tiny sizes [29]. The slight reduction in crystal size is consistent with the XRD analysis.

The BET analysis results (Table 1) validate the SEM observations. The BET surface area of Ag^+ (10^{-2} M) co-catalytic modified powder films exceeds that of pure samples (Table 1). Notably, Ag, 10^{-2}/TP4 powder films exhibit the largest surface area, suggesting potential for the highest photocatalytic activity, compared to pure TP2 and TP4 films, which are expected to have a lower efficiency.

Table 1. Specific surface area of films.

Powder Films	Surface Area, m^2/g
TP2	11
Ag, 10^{-2}/TP2	38
TP4	14
Ag, 10^{-2}/TP4	54

Energy-dispersive X-ray spectroscopy was used to examine the co-catalytically modified TiO_2 films (TP2, TP4) with the highest (10^{-2} M) silver content to determine the presence of Ti, O, and Ag (Figure 3). Peaks of varying intensities representing oxygen, silver, and titanium atoms are evident. The approximate weight percentage of Ag is around 5 wt%. The presence of Si is attributed to the glass substrates on which the nanostructured materials are deposited. The lack of impurity peaks in the EDS spectrum signifies the high purity of the produced powder films, indicating the successful production of high-purity Ag modified TiO_2 material photo-fixed under ultraviolet light.

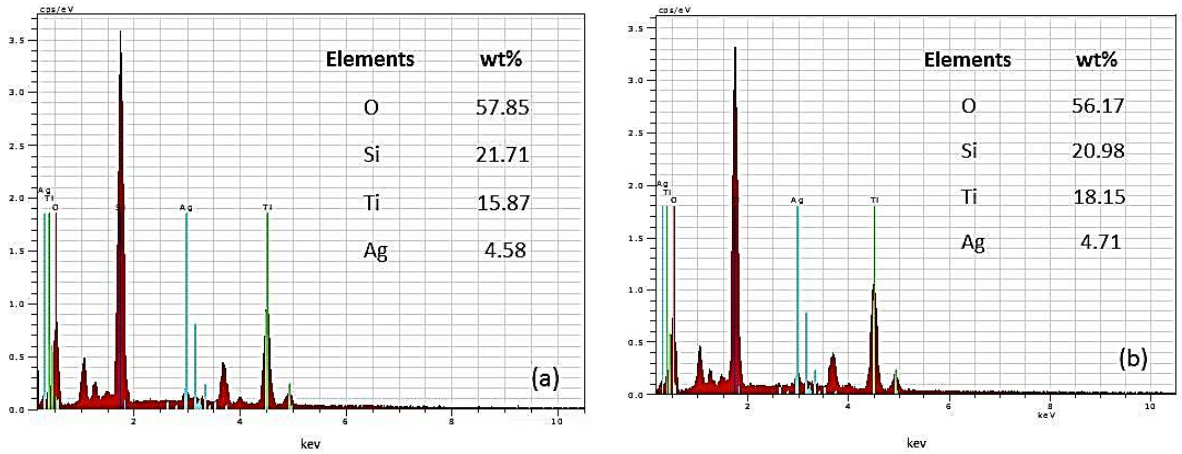

Figure 3. EDS spectra of (**a**) Ag, 10^{-2}/TP2 and (**b**) Ag, 10^{-2}/TP4 films.

The crystal structure of the produced pure and silver (10^{-2} M) modified film is determined using X-ray diffraction (Figure 4). The primary phase of the pure semiconductor films (TP2, TP4) is anatase, evidenced by intense diffraction peaks at 25.45, 38.35, 48.35, 53.91, 55.07, and 63.2°, corresponding to (101), (004), (200), (105), (211), and (204), respectively, and matching the standard JCPDS card (96-500-0224). Both pure TiO_2 (TP2, TP4) films exhibit well-defined peaks, indicating a crystalline film free of impurities. The photo-fixation of silver does not alter the anatase structure in Ag/TP2 and Ag/TP4; however, at a concentration of 10^{-2} M, additional peaks at 38.46, 45.86, and 64.72° emerge, corresponding to planes (111), (200), and (220) of the metallic form of Ag (JCPDS 96-901-3048). Similar patterns have been reported for TiO_2 co-catalytically modified with silver ions [30]. A modest reduction in the TP2 photocatalyst's diffraction peak at (101) is noted, suggesting a suppressed grain growth [31]. The average crystallite size of the samples, determined using the Debye Scherrer formula (Table 2), reveals smaller crystalline sizes in TP4 and Ag/TP4, compared to those in TP2 and Ag/TP2. This reduction correlated with an increase in non-ionic surfactant molecular weight. Enhanced crystallinity and reduced particle size have a significant relationship with high catalytic efficiency, indicating a potential for efficient generation of e^- on the photocatalyst surface [32]. This suggests that carefully regulated grain growth could enhance photocatalytic activity under light irradiation.

The XRD data indicate that photo-fixation with Ag^+ (10^{-2} M) does not significantly alter crystal size. Additionally, co-catalytic modification results in a drop in the intensity of the TiO_2 peaks, observed in both the Ag/TP2 and Ag/TP4 diffractograms. Crystalline lattice parameters remain almost constant, with a slight decrease in the average crystallite size following photo-fixation (Table 2).

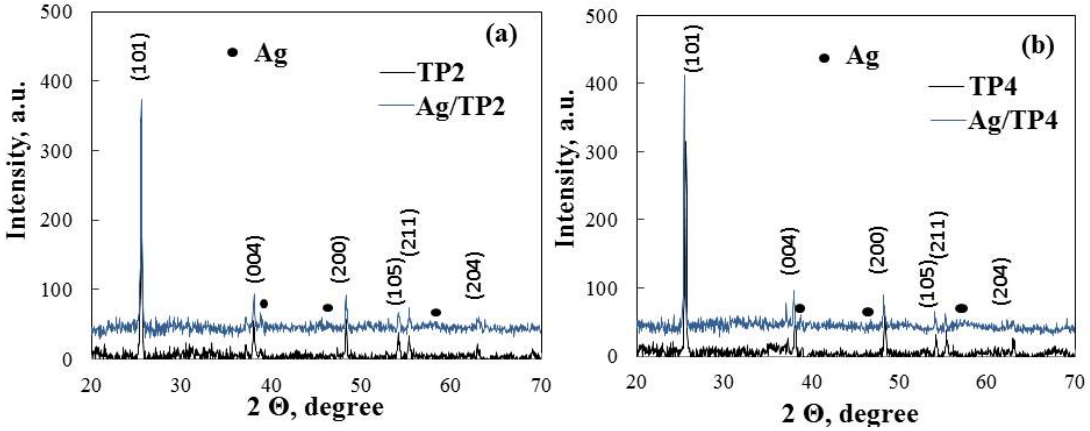

Figure 4. XRD patterns of (**a**) Ag, 10^{-2}/TP2 and (**b**) Ag, 10^{-2}/TP4 powder films.

Table 2. Crystallite size and parameters of the crystalline lattice of pure and Ag^+ (10^{-2} M) modified TiO_2 films.

Powder Films	Crystallite Size, nm	Parameters of the Crystalline Lattice, Å	Microstrains, a.u.
TP2	42.6	a, b: 3.7067 c: 9.5136	0.9×10^{-4}
Ag, 10^{-2}/TP2	39.5	a, b: 3.7055 c: 9.3853	0.7×10^{-4}
TP4	38.5	a, b: 3.7058 c: 9.6332	0.8×10^{-4}
Ag, 10^{-2}/TP4	36.3	a, b: 3.7136 c: 9.3809	0.6×10^{-4}

Silver co-catalytically modified films retain their anatase structure, as evidenced by calculated lattice parameters closely resembling those of TiO_2. Furthermore, the c-axis lattice parameter is used to calculate the microstrain of the films, revealing a positive value indicative of tensile strain. Modified films exhibit slightly larger tensile strain, compared to TiO_2.

3.2. Photocatalytic Evaluation

Sol-gel (ZnO, TiO_2) and powder (ZnO) films were created in our three earlier studies [33–35]. Both the silver ion modification method and the photo-fixation method are the same. For four hours, we broke down the medication (paracetamol) and organic dyes (Malachite green and methylene blue) in these three publications when exposed to UV and visible light. Using surfactants with two distinct molecular weights, we photo-fixed silver ions onto films from commercial TiO_2 powder in this paper. Due to the pollutants' shorter 3 h half-lives under UV and visible light, this approach is more successful. The contaminants were Malachite green and methylene blue.

As visible light is known to cause photolysis in colored dyes, a control experiment was carried out to estimate the dye removal rates in the absence of a photocatalyst. The results are shown in Figure 5 for both MB and MG, indicating an upwards of 13.2% Malachite green lost due to photolysis within 4 h and a higher rate of 18% for Methylene blue, which is known to act as a photosensitizer and thus is more prone to photolysis.

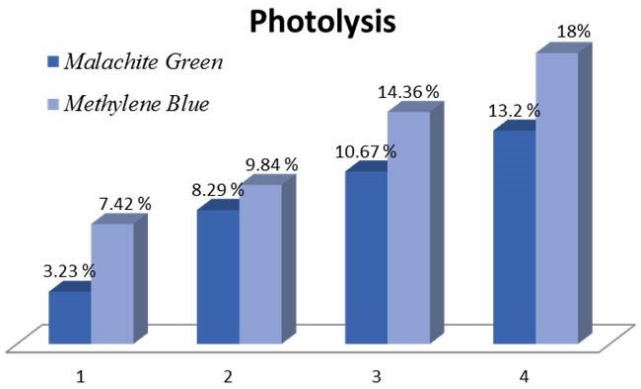

Figure 5. Photolysis rates for MG and MB.

Additionally, a dark phase adsorption experiment with both dyes was carried out for the pristine catalysts (TP2, TP4). The decrease in the concentration of dyes in both cases was ~15% of the initial 10 ppm. The data from adsorption and photolysis are included in Figures 6 and 7.

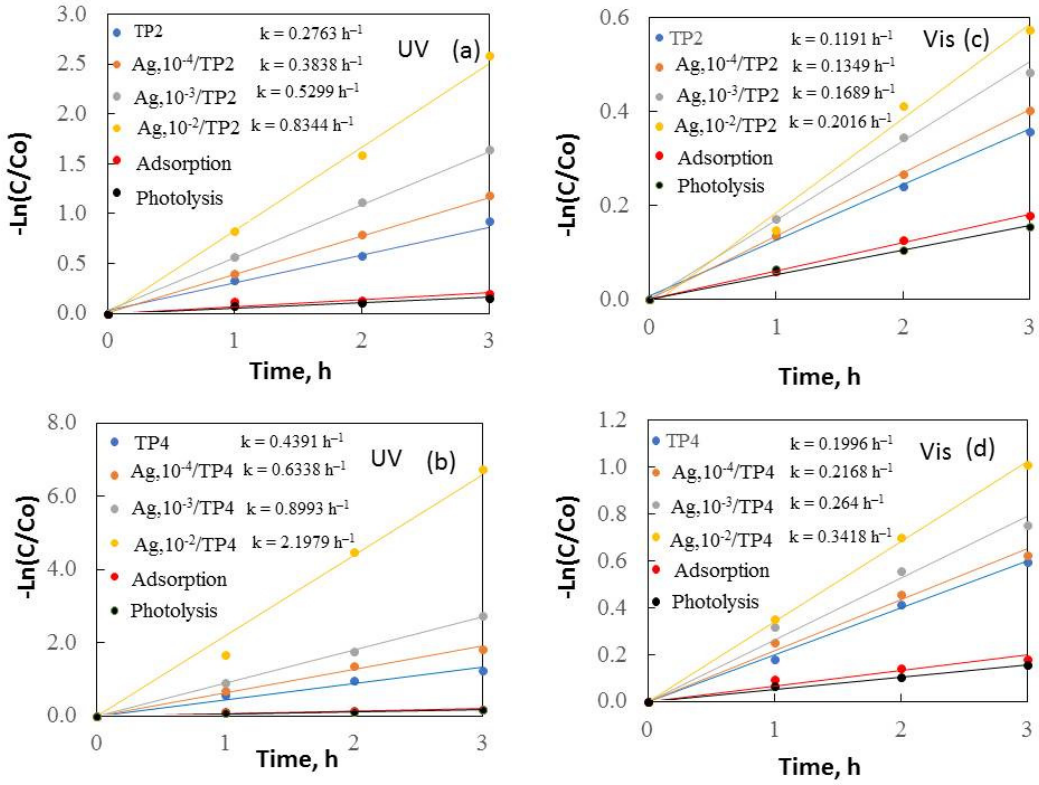

Figure 6. Kinetics of removal of malachite green under UV (**a**,**b**) and visible (**c**,**d**) light.

Figures 6 and 7 depict $-\mathrm{Ln}(C/C_o)$ plotted against irradiation time, revealing a constant reaction rate for the samples. It is noticeable that the increased surfactant molecular mass and silver concentrations enhanced the samples' photocatalytic behavior under both ultraviolet and visible light.

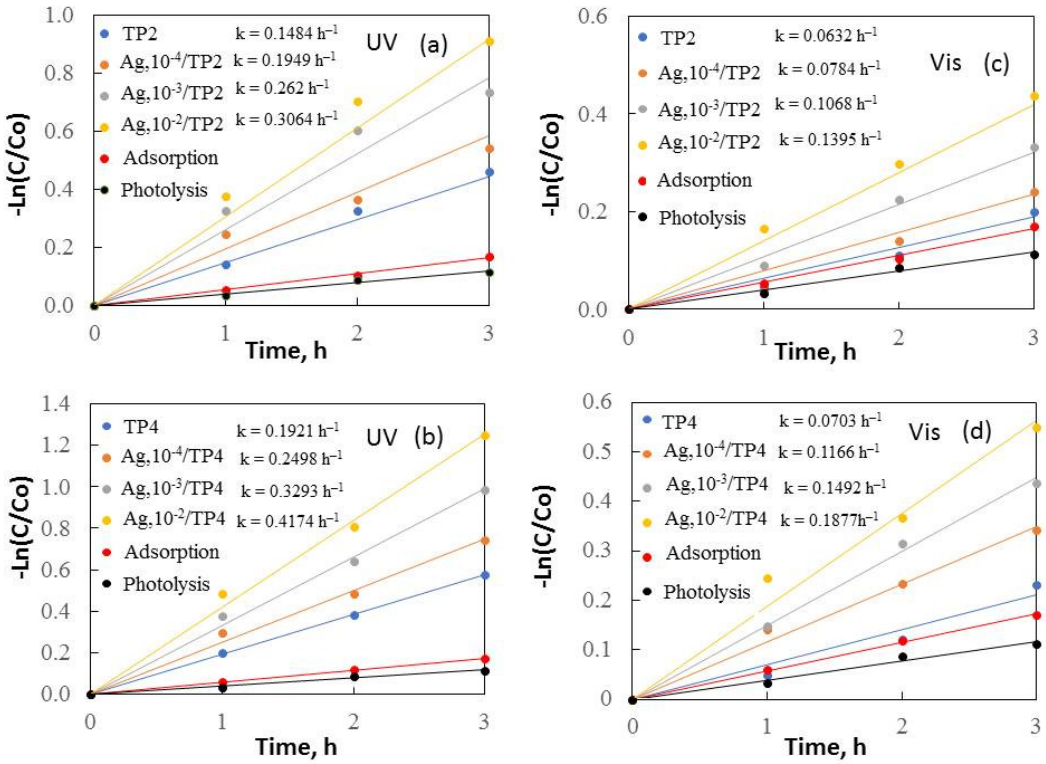

Figure 7. Kinetics of removal of methylene blue under UV (**a**,**b**) and visible (**c**,**d**) light.

The results demonstrate that TP4 films have activity compared to TP2. The smaller crystallite size (38.5 nm), and greater surface area (14 m^2/g) of TP4 facilitate, faster degradation of organic dyes. The TP4 films displayed better photocatalytic efficiency than the TP2 samples, attributed to the increasing molecular weight of the surfactant and the improved morphology, crystalline size, and grain growth of the samples. Increasing the surface area typically leads to greater substrate adsorption, enhancing electron and hole reaction with the substrates. However, a larger surface area can also accelerate the e^-/h^+ recombination, reducing the reaction rate. Thus, the specific surface area influences photoactivity; a larger surface area photocatalyst is preferable when surface reaction dominates recombination, and vice versa.

Additional photocatalytic tests were conducted to assess the impact of the Ag^+ concentration (10^{-4}–10^{-2}M range) on the co-catalytic modification of TP2 and TP4 films during the photocatalytic decolorization process of dyes. The activity of silver photo-fixed samples surpasses that of TP2 and TP4 films, validated by the rate constants. Silver photo-fixation significantly enhances the efficacy of both TiO_2 films, leading to an additional increase in rate constants, observed in both the TP2 and TP4 samples. Our tests reveal that the presence of silver enhances the degradation of dyes under light exposure. Light absorption by TiO_2 excites electrons from the valence band to the conduction band. Co-catalytic modification with silver enhances TiO_2 activity for MG and MB photodecomposition by trapping electrons from the conduction band onto Ag [17], which produce superoxide radicals [36]. Simultaneously, photoinduced holes in the TiO_2 valence band react with surface-attached H_2O or OH^- to produce $OH^\bullet$ radicals, potent oxidants crucial for decomposing organic pollutants. Utilizing silver photo-fixed TiO_2 improves photocatalytic activity using by enhancing photo-induced charge carrier separation and delaying electron-hole pair recombination [30]. Silver acts as an electron trap, absorbing e^- from the TiO_2 conduction band and transferring them to O_2 to form superoxide radicals. Water molecules react with the remaining photogenerated holes on TiO_2 to produce hydroxyl radicals, facilitating the effective degradation of dyes dissolved in distilled water. Figure 8 illustrates a potential mechanism for degrading organic dyes using pure and silver photo-fixed films.

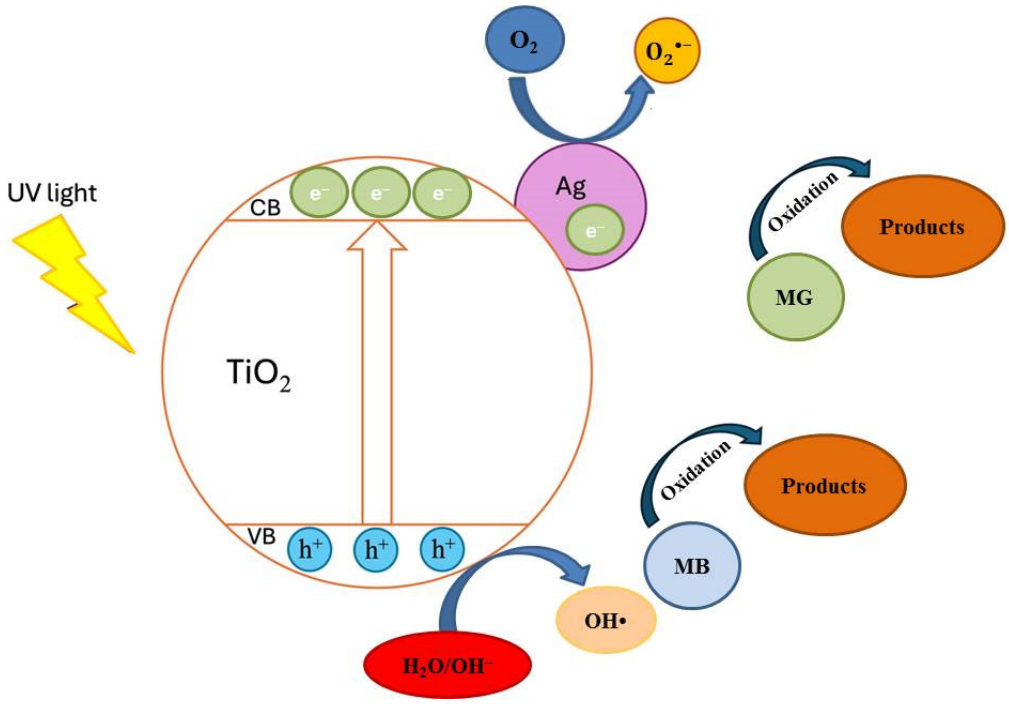

Figure 8. The potential mechanism of photocatalysis.

Due to the creation of stable intermediates by the reaction of $OH^{\bullet}$ with triarylmethane dye (C=C bond), the pure and silver co-catalytically modified films exhibited a faster degradation of MG compared to that of MB. The literature [37,38] describes the processes by which $OH^{\bullet}$ causes degradation of Methylene blue and Malachite green, a process in which, according to Houas et al. [37], the $OH^{\bullet}$ first cleaves the S+=C bond, which causes the central heterocyclic part to undergo a ring-opening reaction, in the case of MB. Similarly, Ju et al. [38] revealed that for the MG case, the first stage of dye decomposition involves a radical attack on the C atom (central), changing it into a Malachite green carbinol base and causing the pollutant to degrade once more. After considering the aforementioned logic, it can be said that the $OH^{\bullet}$-facilitated attack on the S atom may be the cause of the Malachite green's quicker degradation observed in this investigation, attributed to an increase in the electron density.

Sustaining consistently high photocatalytic efficiency throughout the repeated usage of a photocatalyst is crucial for its applicability in environmental applications. Therefore, photocatalytic experiments are also conducted to test the cycling stability of the two best catalysts (TP4 and Ag, 10^{-2}/TP4) for the degrading MG and MB under UV illumination. Figure 9 illustrates the findings of an investigation into powder regeneration and repurposing, indicating a progressive decline in the catalytic quality with each cycle. After three cycles, both dyes' photocatalytic decomposition decreased by approximately 2% for each of the TP4 and Ag, 10^{-2}/TP4 catalysts. Nonetheless, the co-catalytically modified nanostructures continued to have high photo-catalytic activity after three cycles of experiments.

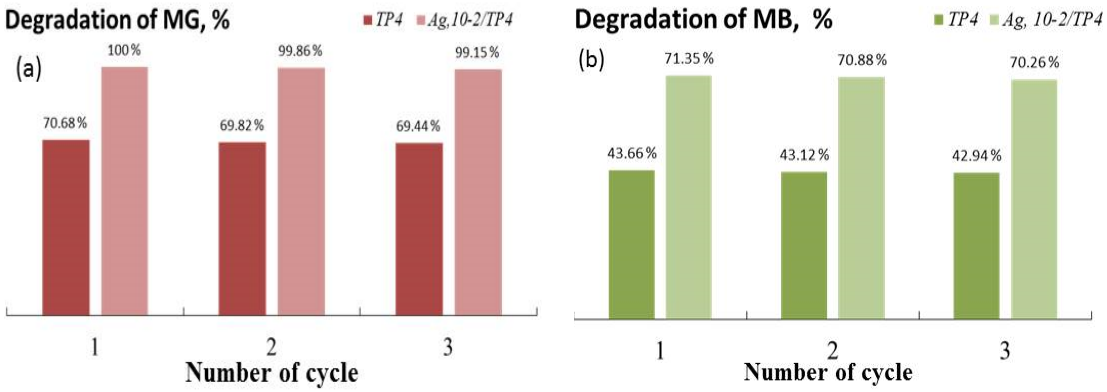

Figure 9. Photostability of TP4 and Ag, 10^{-2}/TP4 on the decomposition of MG (**a**) and MB (**b**).

The presence of silver in the two dye solutions before, during, and after photocatalysis was tested to check for co-catalyst leeching from the catalysts. From the provided photocatalytic experiments, it was determined that the limit of detection (LOD) for samples with MG was 0.0014 mg/L and for MB was 0.0071 mg/L. Interestingly, there is no residual Ag from the photocatalysis of both dyes using visible light (concentrations measured were below the LOD value). In all studied solutions of Methylene blue, the silver measured is below the LOD of the analytical procedure used at the 1st, 2nd, 3rd, or 4th h Residual silver is found after the photocatalytic decomposition of MG under UV light using TP2 and Ag, 10^{-2}/TP2 films (from 0.0076 ± 0.0005 to 0.014 ± 0.001 mg/L), as well as TP4 and Ag, 10^{-2}/TP4 (0.0076 ± 0.0005 to 0.013 ± 0.001 mg/L), which could be ascribed to a non-homogenous distribution of silver.

Finally, the photocatalytic decomposition of dyes in tap water is also tested (Figure 10). Compared to pure films, the Ag-modified films exhibited higher activity; with Ag, 10^{-2}/TP4 film demonstrating the highest activity in photocatalysis in both types of water. The pure and Ag-modified samples exhibited a lower rate of pollutant degradation in distilled water due to variations in the pH levels. Despite slight differences, both waters have different pH values, with tap water (pH = 7.39) having a marginally higher pH than that of distilled water (pH = 6.5). This indicates a higher concentration of OH^- in tap water, resulting in more $OH^\bullet$ and thus more effective degradation of pollutants.

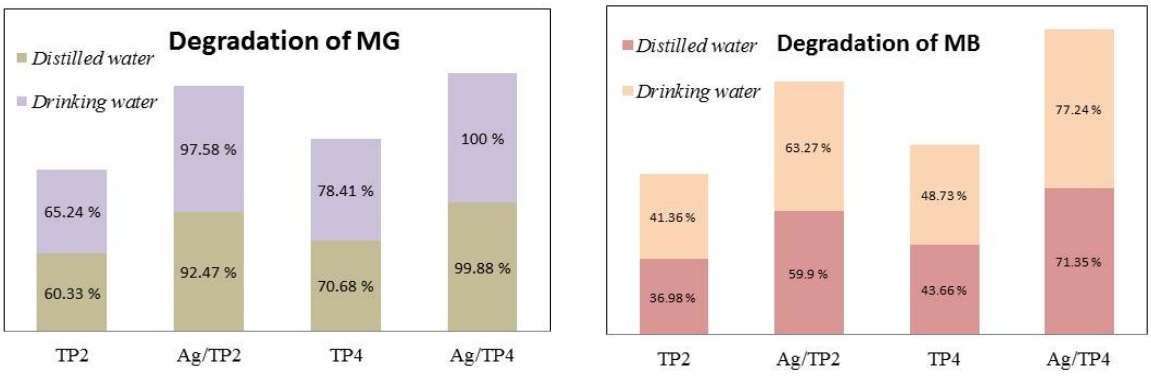

Figure 10. Degradation of the dyes in distilled and tap waters under UV illumination.

The TOC percentages for dye mineralization in tap and distilled water were determined (Figure 11). In tap water, TP4 showed higher TOC conversion rates compared to those of TP2 for both MG and MB, while in distilled water, similar trends are observed. The introduction of Ag^+ into TiO_2 increased the TOC conversion rates, with higher rates observed for films with higher concentrations of silver and surfactant molecular mass. However, comparing the TOC analysis to the UV–vis spectroscopy revealed lower val-

ues, indicating the involvement of complex intermediate steps and products in the dye breakdown process [39,40]. These intermediate products, upon interaction with with $OH^{\bullet}$ produced during photocatalysis, exhibit unique oxidation potentials.

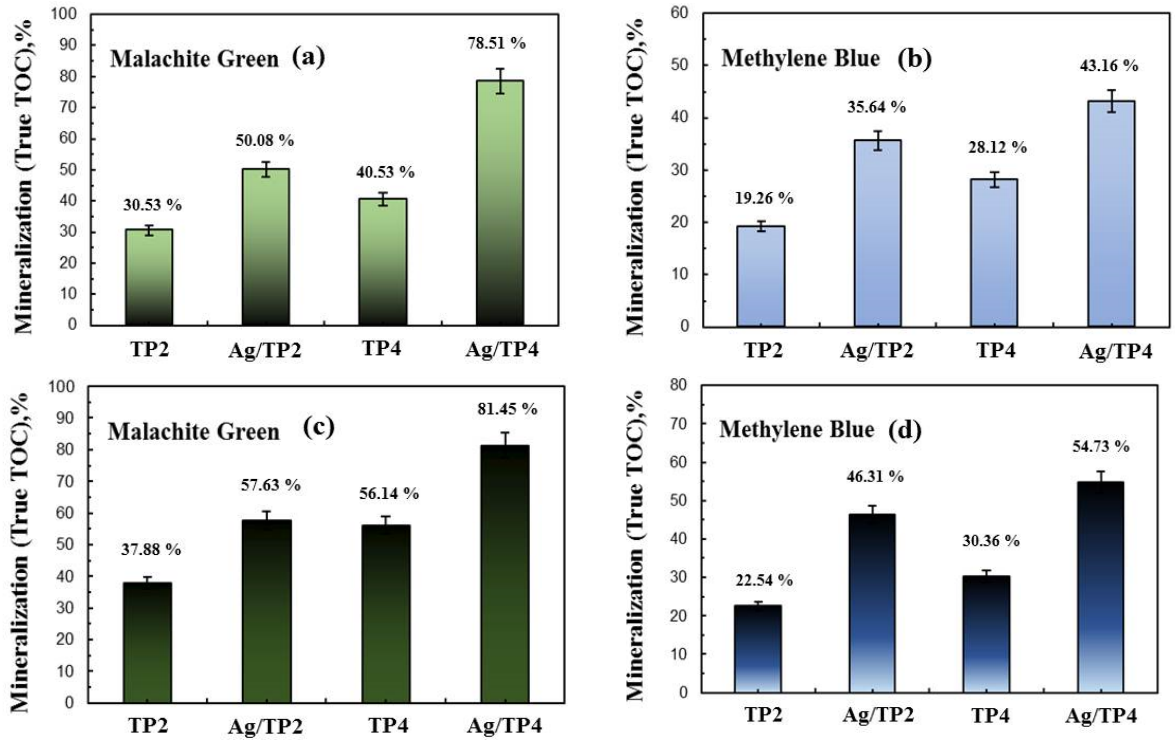

Figure 11. TOC mineralization of Malachite green and Methylene blue in distilled (**a**,**b**) and drinking (**c**,**d**) water.

4. Conclusions

In conclusion, TiO_2 films produced via a dip-coating method with the addition of surfactants (PEG2000 and PEG4000) showed enhanced photocatalytic activity when Ag^+ was photo-fixed under UV light. Films with higher concentrations of silver and surfactant molecular mass demonstrated the highest percentages of dye degradation under light exposure. The system's improved photocatalytic efficiency and the beneficial effects of Ag^+ make it a promising option for pollutant (dye or pharmaceutical drug) degradation, contributing to the development of efficient and environmentally friendly wastewater treatment techniques under ultraviolet light and sunlight.

Author Contributions: Conceptualization N.K.; methodology, N.K.; investigation, N.K., D.I. and E.M.; writing—original draft preparation, N.K. All authors have read and agreed to the published version of the manuscript.

Funding: This research was funded by Bulgarian NSF project, grant number: KP-06-N59/11 (KP-06-H59/11).

Institutional Review Board Statement: Not applicable.

Informed Consent Statement: Not applicable.

Data Availability Statement: Data are contained within the article.

Acknowledgments: N.K. and D.I. are thankful to the Bulgarian NSF project KP-06-N59/11 (KP-06-H59/11). E. M. is grateful to INFRAMAT.

Conflicts of Interest: The authors declare no conflicts of interest.

References

1. Vega-Mendoza, M.; Luévano-Hipólito, E.; Torres-Martínez, L. Design and fabrication of photocatalytic coatings with α/β-Bi_2O_3 and recycled-fly ash for environmental remediation and solar fuel generation. *Ceram. Int.* **2021**, *47*, 26907–26918. [CrossRef]
2. Luévano-Hipólito, E.; Torres-Martínez, L.; Vega-Mendoza, M.; Treviño-Garza, M.; Vázquez-Guillén, J.; Báez González, J.; Rodríguez-Padilla, C. Photocatalytic performance of alkali-activated materials functionalized with β-Bi_2O_3/$Bi_2O_2CO_3$ heterostructures for environmental remediation. *Constr. Build. Mater.* **2022**, *320*, 126205. [CrossRef]
3. Rodríguez-Alfaro, L.; Torres-Martínez, L.; Treviño-Garza, M.; Vázquez-Guillén, J.; Rodríguez-Padilla, C.; Luévano-Hipólito, E. Design and fabrication of photocatalytic magnesium oxychloride cement with improved moisture stability: A step towards sustainable construction. *Constr. Build. Mater.* **2024**, *414*, 134804. [CrossRef]
4. Luévano-Hipólito, E.; Torres-Martínez, L.; Rodríguez-González, E. Recycling Waste Materials to Fabricate Solar-Driven Self-Cleaning Geopolymers. *Waste Biomass Valorization* **2024**, *15*, 2833–2843. [CrossRef]
5. Dang, Z.; Yan, B.; Wang, D.; Guo, H.; Zhao, W.; Li, H. One-step preparation of cast stone from TBFS: Dual effects of TiO_2 content on glass network and precipitation behavior. *J. Non-Cryst. Solids* **2024**, *629*, 122884. [CrossRef]
6. Limsakul, S.; Mahatnirunkul, T.; Phromma, C.; Chomtong, T.; Cholnakasem, N.; Yimklan, S.; Ruankham, P.; Siyasukh, A.; Chimupala, Y. Novel physical sunscreen from one-dimensional TiO_2 nanowire: Synthesis, characterization and the effects of morphologies and particle size for use as a physical sunscreen. *Nano-Struct. Nano-Objects* **2023**, *35*, 101027. [CrossRef]
7. Rajaitha, P.M.; Hajra, S.; Sahu, M.; Mistewicz, K.; Toroń, B.; Abolhassani, R.; Panda, S.; Mishra, Y.; Kim, H. Unraveling highly efficient nanomaterial photocatalyst for pollutant removal: A comprehensive review and future progress. *Mater. Today Chem.* **2022**, *23*, 100692. [CrossRef]
8. Gopinath, K.; Madhav, N.; Krishnan, A.; Malolan, R.; Rangarajan, G. Present applications of titanium dioxide for the photocatalytic removal of pollutants from water: A review. *J. Environ. Manage.* **2020**, *270*, 110906. [CrossRef]
9. Al-Mamun, M.; Kader, S.; Islam, M.; Khan, M. Photocatalytic activity improvement and application of UV-TiO_2 photocatalysis in textile wastewater treatment: A review. *J. Environ. Chem. Eng.* **2019**, *7*, 103248. [CrossRef]
10. Basavarajappa, P.; Patil, S.; Ganganagappa, N.; Reddy, K.; Raghu, A.; Reddy, C. Recent progress in metal-doped TiO_2, non-metal doped/codoped TiO_2 and TiO_2 nanostructured hybrids for enhanced photocatalysis. *Int. J. Hydrogen Energy* **2020**, *45*, 7764–7778. [CrossRef]
11. Lincho, J.; Domingues, E.; Mazierski, P.; Miodyńska, M.; Klimczuk, T.; Zaleska-Medynska, A.; Martins, R.J. Gomes, The role of noble metals in TiO_2 nanotubes for the abatement of parabens by photocatalysis, catalytic and photocatalytic ozonation. *Sep. Purif. Technol.* **2023**, *326*, 124747. [CrossRef]
12. Ferreira, V.; Santos, P.; Silva, C.; Azenha, M. Latest developments on TiO_2-based photocatalysis: A special focus on selectivity and hollowness for enhanced photonic efficiency. *Appl. Catal. A Gen.* **2021**, *623*, 118243. [CrossRef]
13. Kang, S.; Choi, J.; Park, G.; Kim, H.; Hwang, J. A novel and facile synthesis of Ag-doped TiO_2 nanofiber for airborne virus/bacteria inactivation and VOC elimination under visible light. *Appl. Surf. Sci.* **2022**, *599*, 153930. [CrossRef]
14. Rathi, V.; Jeice, A.; Jayakumar, K. Green synthesis of Ag/CuO and Ag/TiO_2 nanoparticles for enhanced photocatalytic dye degradation, antibacterial, and antifungal properties. *Appl. Surf. Sci. Adv.* **2023**, *18*, 100476. [CrossRef]
15. Kanakaraju, D.; Kutiang, F.; Lim, Y.; Goh, P. Recent progress of Ag/TiO_2 photocatalyst for wastewater treatment: Doping, co-doping, and green materials functionalization. *Appl. Mater. Today* **2022**, *27*, 101500. [CrossRef]
16. Saravanan, R.; Manoj, D.; Qin, J.; Naushad, M.; Gracia, F.; Lee, A.; Khan, M.; Gracia-Pinilla, M. Mechanothermal synthesis of Ag/TiO_2 for photocatalytic methyl orange degradation and hydrogen production. *Process. Saf. Environ. Prot.* **2018**, *120*, 339–347. [CrossRef]
17. Chakhtouna, H.; Ouhssain, A.; Kadmiri, I.; Benzeid, H.; Zari, N.; Qaiss, A.; Bouhfid, R. Photocatalytic and bactericidal behaviors of Ag/TiO_2 doped biochar through Ball–milling approach. *J. Photochem. Photobiol. A Chem.* **2023**, *444*, 114971. [CrossRef]
18. Rocha, A.; Reis-Henriques, M.; Galhano, V.; Ferreira, M.; Guimarães, L. Toxicity of seven priority hazardous and noxious substances (HNSs) to marine organisms: Current status, knowledge gaps and recommendations for future research. *Sci. Total Environ.* **2016**, *542 Pt A*, 728–749. [CrossRef]
19. Rehman, A.; Yaqub, S.; Ali, M.; Nazir, H.; Shahzad, N.; Shakir, S.; Liaquat, R.; Said, Z. Effect of surfactants on the stability and thermophysical properties of Al_2O_3 + TiO_2 hybrid nanofluids. *J. Mol. Liq.* **2023**, *391 Pt B*, 123350. [CrossRef]
20. Sun, X.; Yi, M.; Feng, B.; Liu, R.; Sun, L.; Zhai, L.; Cao, H.; Zou, C. Shape-stabilized composite phase change material PEG@TiO_2 through in situ encapsulation of PEG into 3D nanoporous TiO_2 for thermal energy storage. *Renew. Energy* **2021**, *170*, 27–37. [CrossRef]
21. Payormhorm, J.; Chuangchote, S.; Laosiripojana, N. CTAB-assisted sol-microwave method for fast synthesis of mesoporous TiO_2 photocatalysts for photocatalytic conversion of glucose to value-added sugars. *Mater. Res. Bull.* **2017**, *95*, 546–555. [CrossRef]
22. Chen, K.; Li, J.; Wang, W.; Zhang, Y.; Wang, X.; Su, H. Effects of surfactants on microstructure and photocatalytic activity of TiO_2 nanoparticles prepared by the hydrothermal method. *Mater. Sci. Semicond. Process.* **2012**, *15*, 20–26. [CrossRef]
23. Liang, Q.; Liu, X.; Zeng, G.; Liu, Z.; Tang, L.; Shao, B.; Zeng, Z.; Zhang, W.; Liu, Y.; Cheng, M.; et al. Surfactant-assisted synthesis of photocatalysts: Mechanism, synthesis, recent advances and environmental application. *Chem. Eng. J.* **2019**, *372*, 429–451. [CrossRef]
24. Luévano-Hipólito, E.; Martínez-de la Cruz, A.; Yu, Q.; Brouwers, H. Precipitation synthesis of WO3 for NOx removal using PEG as template. *Ceram. Int.* **2014**, *40*, 12123–12128. [CrossRef]

25. Hu, X.; Zhu, Q.; Gu, Z.; Zhang, N.; Liu, N.; Stanislaus, M.; Li, D.; Yang, Y. Wastewater treatment by sonophotocatalysis using PEG modified TiO_2 film in a circular Photocatalytic-Ultrasonic system. *Ultrason. Sonochem.* **2017**, *36*, 301–308. [CrossRef] [PubMed]
26. Zhang, Y.; Han, C.; Zhang, G.; Dionysiou, D.; Nadagouda, M. PEG-assisted synthesis of crystal TiO_2 nanowires with high specific surface area for enhanced photocatalytic degradation of atrazine. *Chem. Eng. J.* **2015**, *268*, 170–179. [CrossRef]
27. An, T.; Liu, J.; Li, G.; Zhang, S.; Zhao, H.; Zeng, X.; Sheng, G.; Fu, J. Structural and photocatalytic degradation characteristics of hydrothermally treated mesoporous TiO_2. *Appl. Catal. A Gen.* **2008**, *350*, 237–243. [CrossRef]
28. Ivanova, D.; Mladenova, E.; Kaneva, N. Photo-fixation of Ag onto TiO_2 powder films improved photocatalytic activity and atomic-absorption determination of residual noble metal in dyes solution. *C. R. Acad. Bulg. Sci.* **2024**, *77*, 20–29. [CrossRef]
29. Tsivadze, A.; Ionova, G.; Mikhalko, V.; Ionova, I.; Gerasimova, G.A. Plasmon properties of silver spherical nanoparticles and films. *Prot. Met. Phys. Chem. Surfaces* **2013**, *49*, 169–172. [CrossRef]
30. Perumal, S.; Gnana, C. Synthesis and characterization studies of solvothermally synthesized undoped and Ag-doped TiO_2 nanoparticles using toluene as a solvent. *Int. J. Eng. Res.* **2014**, *4*, 184–187.
31. Sun, W.; Zhang, S.; Liu, Z.; Wang, C.; Mao, Z. Studies on the enhanced photocatalytic hydrogen evolution over Pt/PEG-modified TiO2photocatalysts. *Int. J. Hydrogen Energy* **2008**, *33*, 1112–1117. [CrossRef]
32. Zhang, M.; Lei, J.; Shi, Y.; Zhang, L.; Ye, Y.; Li, D.; Mu, C. Molecular weight effects of PEG on the crystal structure and photocatalytic activities of PEG-capped TiO_2 nanoparticles. *RSC Adv.* **2016**, *6*, 83366–83372. [CrossRef]
33. Ivanova, D.; Mladenova, R.; Kolev, H.; Kaneva, N. Effect of Ultraviolet Illumination on the Fixation of Silver Ions on Zinc Oxide Films and their Photocatalytic Efficiency. *Catalysts* **2023**, *13*, 1121. [CrossRef]
34. Kaneva, N.; Bojinova, A.; Papazova, K. Enhanced Removal of Organic Dyes Using Co-Catalytic Ag-Modified ZnO and TiO_2 Sol-Gel Photocatalysts. *Catalysts* **2023**, *13*, 245. [CrossRef]
35. Ivanova, D.; Tzvetkov, G.; Kaneva, N. Degradation of Paracetamol in Distilled and Drinking Water via Ag/ZnO Photocatalysis Under UV and Natural Sunlight. *Waters* **2023**, *15*, 3549. [CrossRef]
36. Hamed, N.; Ahmad, M.; Hairom, N.; Faridah, A.; Mamat, M.; Mohamed, A.; Suriani, A.; Nafarizal, N.; Fazli, F.; Mokhtar, S.; et al. Dependence of photocatalysis on electron trapping in Ag-doped flowerlike rutile-phase TiO_2 film by facile hydrothermal method. *Appl. Surf. Sci.* **2020**, *534*, 147571. [CrossRef]
37. Houas, A.; Lachheb, H.; Ksibi, M.; Elaloui, E.; Guillard, C.; Herrmann, M. Photocatalytic Degradation Pathway of Methylene Blue in Water. *Appl. Catal. B Environ.* **2001**, *31*, 145–157. [CrossRef]
38. Ju, Y.; Qiao, J.; Peng, X.; Xu, Z.; Fang, J.; Yang, S.; Sun, C. Photodegradation of malachite green using UV–vis light from two microwave-powered electrodeless discharge lamps (MPEDL-2): Further investigation on products, dominant routes and mechanism. *Chem. Eng. J.* **2013**, *221*, 353–362. [CrossRef]
39. Ray, S.K.; Dhakal, D.; Lee, S. Insight into Malachite Green Degradation, Mechanism and Pathways by Morphology-Tuned α-$NiMoO_4$ Photocatalyst. *Photochem. Photobiol.* **2018**, *94*, 552–563. [CrossRef]
40. Nayak, S.; Das, K.; Parida, K. Indulgent of the physiochemical features of MgCr-LDH nanosheets towards photodegradation process of methylene blue. *J. Colloid Interface Sci.* **2023**, *634*, 121–137. [CrossRef]

Disclaimer/Publisher's Note: The statements, opinions and data contained in all publications are solely those of the individual author(s) and contributor(s) and not of MDPI and/or the editor(s). MDPI and/or the editor(s) disclaim responsibility for any injury to people or property resulting from any ideas, methods, instructions or products referred to in the content.